JOURNAL OF COMPUTATIONAL PHYSICS 68, 202–226 (1987)

A Method for Overcoming the Velocity Space Filamentation Problem in Collisionless Plasma Model Solutions

ALEXANDER J. KLIMAS

Laboratory for Extraterrestrial Physics, Goddard Space Flight Center, Greenbelt, Maryland 20771

Received October 30, 1985; revised: March 31, 1986

A method is introduced for overcoming the velocity space filamentation problem which occurs in solutions of the Vlasov–Maxwell system of equations. This method is shown to introduce no error in the evolution of the Vlasov–Maxwell solutions, to leave the field portion of the solutions unmodified, and to yield velocity-filtered distribution functions which do not carry filamentation in the velocity variable. It is conjectured that the filtered distributions do not develop spatial filamentation as well. It is shown that the method can be applied to the most general three-dimensional, electromagnetic Vlasov–Maxwell model. Several examples are presented in which comparisons between filtered and unfiltered solutions are made. These are numerical solutions of a Fourier–Fourier transformed one-dimensional electron plasma model. In the comparisons, which are favorable, reductions in run time by factors of approximately ten and in necessary machine memory by factors of twenty to thirty are demonstrated.

I. INTRODUCTION

In many situations a collisionless plasma model is an excellent approximation. In that approximation the Vlasov equation describes the evolution of the particle distribution in phase space; it can be written $dF/dt = 0$. The distribution function is unchanged along the characteristics generated by the particle equations of motion. An initial distribution may be mixed by the particle motion into very fine structures in phase space but no relaxation between neighboring elements can occur. Consequently, even a smooth initial distribution can be mixed into a distribution with small scales and large derivatives.

For example, consider an initial value, free streaming (field = 0), solution of the one-dimensional Vlasov equation,

$$\frac{\partial F}{\partial t} + v\frac{\partial F}{\partial x} = 0. \tag{1}$$

If the initial distribution is given by $F(x, v, 0) = G(x, v)$, then the solution of Eq. (1) is $F(x, v, t) = G(x - vt, v)$. The free streaming particle motion shears the initial

0021-9991/87 $3.00

phase space distribution as time increases; initial spatial structure is stretched into fine scale structure in velocity and the derivative of F with respect to velocity,

$$\frac{\partial F}{\partial v} = \left.\frac{\partial G(\zeta, v)}{\partial v}\right|_{\zeta = x - vt} - t\frac{\partial G(x - vt, v)}{\partial x}, \tag{2}$$

grows unbounded.

In principle, this "filamentation" of the distribution function can lead to large derivatives in both the spatial and velocity variables. Denavit [1] has given an example which exhibits this behavior; it is an electron gas trapped in the potential trough of an external electric field. However, in most cases it appears that large velocity derivatives develop first [2].

"Velocity space filamentation" has been a well-known problem in numerical plasma simulations. Early Vlasov simulations [3, 4] based on direct differencing techniques suffered serious degradation after short integration times due to velocity space filamentation. Later Vlasov simulations in which the velocity space was Hermite transformed [5, 6, 7, 8, 9, 10, 11], again because of the velocity derivative growth, were limited to integration times which depended on the number of retained Hermite polynomials [8, 5, 6]. It was found that truncation of the polynomial expansion leads to an apparent numerical instability for larger times which Joyce, Knorr, and Meier [12] showed is actually a recurrence phenomenon associated with the attempt to represent a continuous eigenspectrum by a discrete finite spectrum. Knorr [13] introduced an alternative Vlasov simulation method in which the velocity space is Fourier transformed. This method has been used extensively [14, 15, 16, 10, 17] and has been discussed by Armstrong *et al.* [2] as a solution of the velocity space filamentation problem. However, in their discussion Armstrong *et al.* warned of the loss of information which results when this method is used, as it is usually, on a finite interval in the Fourier variable complementary to the velocity variable. Klimas [17] investigated this issue further using an interval in the Fourier variable which expanded with the flow of information and showed that the formation of significant velocity space filamentation quickly leads to an intractable computational problem unless the loss of information is accepted. The impact of this loss of information on the accuracy of the computed solution is unknown. It is clear if echo effects [18, 19] or velocity space filamentation are important features of the solution then the loss of information must be serious.

Various attempts have been made to overcome the velocity space filamentation problem. Grant and Feix [5, 6] added a weak Fokker–Planck collision term to the right side of the Vlasov equation to relax the fine velocity space structures which develop otherwise. Joyce *et al.* [12] and Knorr [11] imposed small imaginary parts on the eigenvalues in their Hermite polynomial expansions to damp away the recurrence phenomena associated with truncation of the expansions. Joyce *et al.* [12] also considered adding a collision term to the Vlasov equation to damp the recurrence phenomena. Cheng and Knorr [20] introduced a filtration method for removing the filamentation from the velocity distribution. They periodically stop-

ped their computation, filtered the velocity distribution through a convolution integration with a filter function which was chosen to leave the low order moments of the distribution, of physical interest, unaffected, and then restarted their computation using the filtered distribution for new initial data. All of the above are selective mechanisms which act most strongly on those portions of the velocity distribution with large velocity derivatives to reduce the derivatives; they can extend the validity of computed solutions somewhat, but eventually the errors which these methods introduce accumulate and then dominate.

The method which is investigated in this paper for overcoming the velocity space filamentation problem was first suggested by Kellogg [4]; it is related to the filtration method of Cheng and Knorr [20]. This method is different in that it introduces no error. A filtered distribution, similar to that of Cheng and Knorr, is introduced. Then, the equations which govern the evolution of the filtered distribution are constructed from the Vlasov–Maxwell equations which govern the unfiltered distribution. With an appropriate choice of filter function, these "filtered equations" are only slightly more complicated to solve numerically and, given the lack of filamentation in their solutions, these computations actually can be done considerably faster. The filtered Vlasov–Maxwell equations differ from the unfiltered ones only in the addition of a single differential term on the right side of the Vlasov equation which is reminiscent of but quite unrelated to the collision terms which have been added there in the past; there are no other modifications. This statement holds for any number of dimensions and for the full set of Maxwell's equations governing the most general electromagnetic field. The field which is computed from the filtered equations is identical to that which is ordinarily computed from the unfiltered equations; there is no loss of information concerning the field evolution. The price that is paid is a loss of resolution in the velocity distribution. It is important to remember, however, that this loss of resolution does not in any way affect the evolution of the solution. The application of this method can be thought of as the act of viewing the evolution of the exact solution through a plasma detector which has less than perfect resolution in velocity; the view may be imperfect but that does not change the solution.

In this paper, the method for overcoming the velocity space filamentation problem is introduced, some of its properties are discussed, and several examples of its application to numerical computations are given. For simplicity, all of this is in terms of a one-dimensional electron plasma model discussed previously by Klimas [17] and Klimas and Cooper [21]. As mentioned above, the method is completely generalizable up to, and including, the three dimensional electromagnetic case; the generalization is given in Appendix A.

II. The Method

Consider the following collisionless, one-dimensional, model for an electron plasma:

$$\frac{\partial F}{\partial \tau} + v\frac{\partial F}{\partial x} - E(x,\tau)\frac{\partial F}{\partial v} = 0, \tag{3}$$

$$\frac{\partial E}{\partial x} = 1 - \int_{-\infty}^{\infty} dv\, F(x, v, \tau), \tag{4}$$

and

$$\frac{\partial E}{\partial \tau} = \int_{-\infty}^{\infty} dv\, vF(x, v, \tau) - U. \tag{5}$$

In this model there is assumed a passive neutralizing ion background with uniform normalized density, represented by the 1 in Eq. (4), and with possibly a uniform average ion flow speed, represented by the U in Eq. (5). The necessity of Eq. (5), as well as the close relationship between solutions of this system of equations and those of the more familiar Vlasov–Poisson system comprised of the first two of the above equations, are discussed by Klimas [17] and by Klimas and Cooper [21]. The filamentation problem is unchanged by the addition of Eq. (5).

The method which will be considered here for overcoming the filamentation problem is based on the introduction of the filtered distribution function,

$$\bar{F}(x, v, \tau) = \int_{-\infty}^{\infty} dv'\, £(v - v')\, F(x, v', \tau), \tag{6}$$

with the specific choice for the filter function,

$$£(v) = (1/v_0\sqrt{2\pi})\, e^{-(1/2)(v/v_0)^2}, \tag{7}$$

in which v_0 is a constant parameter which controls the width of the filter and therefore the velocity resolution which is retained in $\bar{F}$. Of course, in the limit $v_0 = 0$, $\bar{F} = F$. Other, more general, filter functions have been suggested by Cheng [22] and by Knorr [23]; these are discussed briefly in Appendix B. The discussion in this paper will be limited to the gaussian filter function. The equations which $\bar{F}$ satisfies can be constructed by applying the filtering operation defined above to Eqs. (3)–(5) using the filter function defined in Eq. (7). The necessary calculations, generalized to the three dimensional electromagnetic case, are done in Appendix A. The results for the one-dimensional electron plasma model under consideration here are,

$$\frac{\partial \bar{F}}{\partial \tau} + v\frac{\partial \bar{F}}{\partial x} - E(x,\tau)\frac{\partial \bar{F}}{\partial v} = -v_0^2\frac{\partial^2 \bar{F}}{\partial x\, \partial v}, \tag{8}$$

$$\frac{\partial E}{\partial x} = 1 - \int_{-\infty}^{\infty} dv\, \bar{F}(x, v, \tau), \tag{9}$$

and

$$\frac{\partial E}{\partial \tau} = \int_{-\infty}^{\infty} dv\, v\, \bar{F}(x, v, \tau) - U. \tag{10}$$

It will be shown shortly that solutions of Eqs. (8)–(10) for $\bar{F}$ cannot contain velocity space filamentation if v_0 is properly chosen. Thus, the solution of the filamentation problem which is proposed is to look for filtered solutions of Eqs. (8)–(10) in lieu of unfiltered solutions of Eqs. (3)–(5). If the initial data (and possible boundary data) for the filtered and unfiltered solutions are related to each other by Eq. (6), then the filtered and unfiltered solutions will always be related to each other through Eq. (6) with each solution satisfying its respective system of equations. The fact that $\bar{F}$ is computed in no way changes the evolution of F. Thus, $\bar{F}$ can always be considered a filtered look at the exact solution. No error is introduced into the solution for F.

Some important properties of the filtered solutions are discussed in the following:

(a) *An a priori Bound on* $\partial\bar{F}/\partial v$.

From Eq. (6), the derivative with respect to velocity of $\bar{F}$ can be written,

$$\frac{\partial \bar{F}(x, v, \tau)}{\partial v} = \int_{-\infty}^{\infty} dv' \frac{\partial \pounds(v - v')}{\partial v} F(x, v', \tau). \tag{11}$$

If $\bar{F}_m$ is the maximum value of $\bar{F}$ which is imposed on the solution in the initial or boundary data, then,

$$\begin{aligned} \left|\frac{\partial \bar{F}(x, v, \tau)}{\partial v}\right| &\leqslant \bar{F}_m \int_{-\infty}^{\infty} dv' \left|\frac{\partial \pounds(v')}{\partial v'}\right| = 2\bar{F}_m \int_{-\infty}^{0} dv' \frac{\partial \pounds(v')}{\partial v'} \\ &= 2\bar{F}_m \pounds(0) = \sqrt{2/\pi}\,\frac{\bar{F}_m}{v_0}. \end{aligned} \tag{12}$$

Thus, it is possible to make an estimate of the maximum velocity derivative which will occur in the solution and choose the velocity grid spacing accordingly. It is also possible to adjust the maximum derivative, and the grid spacing, through adjustments to the parameter v_0. In some situations it may be advantageous to choose a large v_0 and then use a coarse velocity grid. In such situations little may be learned about the distribution function because of the severe smoothing imposed on it. However, the computation would run relatively quickly with less real storage requirements and it would still yield the correct field evolution. In other situations it may be desirable to choose v_0 somewhat smaller so that filamentation is removed but the basic shape and evolution of the distribution is left.

(b) *The Field Solution is Invariant to Filtering*

With the symmetric and unit weight ($\int dv\, \pounds(v) = 1$) filter function defined by Eq. (7), the zeroth and first moments of F and $\bar{F}$ are identical, i.e.,

$$\int_{-\infty}^{\infty} dv\, F(x, v, \tau) = \int_{-\infty}^{\infty} dv\, \bar{F}(x, v, \tau) \tag{13}$$

and

$$\int_{-\infty}^{\infty} dv\, v\, F(x, v, \tau) = \int_{-\infty}^{\infty} dv\, v\, \bar{F}(x, v, \tau). \tag{14}$$

Therefore, the charge and current densities computed using either F or $\bar{F}$ are identical and the field solutions, which depend on the distribution function only through the charge and current densities, are the same for the unfiltered solution and any of the filtered solutions with various v_0.

(c) *Spatial Filamentation May Not Develop*

When acting on an arbitrary free streaming function of the type discussed in the introduction the second order differential term on the right side of Eq. (8) behaves like a diffusion operator with a time dependent diffusion coefficient; i.e.,

$$\begin{aligned} -v_0^2 \frac{\partial^2 \Psi(x - v\tau)}{\partial x\, \partial v} &= \frac{v_0^2}{\tau} \frac{\partial^2 \Psi(x - v\tau)}{\partial v^2} \\ &= v_0^2\, \tau \frac{\partial^2 \Psi(x - v\tau)}{\partial x^2}. \end{aligned} \tag{15}$$

This behavior leads to rapid relaxation of the free streaming solution of the filtered Eqs. (8)–(10) toward a spatially uniform state with no velocity space filamentation. For example, consider a solution which contains a single spatial Fourier mode. Let $\bar{F}(x, v, 0) = \bar{G}(x, v) = \bar{G}(k, v) \exp(ikx)$. Then,

$$\bar{F}(x, v, \tau) = \bar{G}(k, v - ikv_0^2\tau, 0)\, e^{ik(x - v\tau) - (1/2)(v_0 k\tau)^2}. \tag{16}$$

In the limit $v_0 = 0$ this expression reduces to the standard free streaming solution with its unbounded velocity derivative. However, when $v_0 \neq 0$ the rapid gaussian decay with increasing τ prevents the unbounded growth of the derivative. Note that this gaussian decay is faster for larger k. In the filtered free streaming solution short spatial wavelengths decay away rapidly leaving a smooth solution in position as well as velocity. At least in the linear approximation, the more general solution with $E \neq 0$ can be considered the superposition of the free streaming solution and the usual linear approximation which will generally Landau damp for short spatial wavelengths. Thus, it is conjectured solutions which are filtered in velocity and which, as has been shown above, can be made as smooth as necessary in the velocity variable will also remain smooth in the spatial variable.

III. Application to the Fourier–Fourier Transformed Equations

In this section application of the method for overcoming velocity space filamentation to the Fourier–Fourier transformed version of Eqs. (8)–(10) will be discussed.

Knorr [13] originally introduced the Fourier–Fourier transformation method in a discussion of the one-dimensional Vlasov–Poisson system of equations. Klimas [17] later applied this method to the more general Vlasov–Maxwell system, Eqs. (3)–(5) above. Application of this method to the filtered system, Eqs. (8)–(10), yields (in the notation of Klimas),

$$\frac{\partial \bar{K}_m}{\partial \tau} + m \frac{\partial \bar{K}_m}{\partial v} = \nu(A_{m,n} - \varepsilon m \delta_{m,n})\, \bar{K}_n + \bar{\sigma}_m, \tag{17}$$

with

$$\begin{aligned} A_{m,n}(\tau) &= \frac{\bar{K}_{m-n}(0, \tau)}{m-n} \qquad (m \neq n) \\ &= 0 \qquad\qquad\qquad (m = n) \end{aligned} \tag{18}$$

and

$$\varepsilon = \frac{1}{v_0^2} = (\pi v_0)^2, \tag{19}$$

in which the sum on the index, n, is implied. This is an infinite system of coupled, hyperbolic, semilinear, first order partial differential equations shown here for the mth spatial Fourier mode which is a function of time, τ, and of velocity space wave number, ν. In the limit $\varepsilon = 0$ this system reduces to the system given by Klimas [17] for the unfiltered case. Normally, initial value solutions are sought with the input function $\bar{\sigma}_m(\nu, \tau)$ determined by possible nonperiodic boundary conditions on the spatial interval under consideration.

From Eq. (17), the characteristics of the Fourier–Fourier transformed system of equations are straight lines on the (ν, τ)-plane; for initial value solutions these are given by $\nu_m(\tau) = \nu_m(0) + m\tau$. The development of velocity space filamentation can be understood on the basis of these characteristics. An initial distribution which is smooth in velocity will not contain large values of ν in its Fourier transform; its Fourier transform can be considered effectively a compact function of ν about $\nu = 0$. But, with increasing τ the $\bar{K}_m$ can propagate from the vicinity of $\nu = 0$ to large values of ν along the characteristics defined above, this propagation being particularly rapid for the higher index (shorter wavelength) modes. For example, the free streaming solution in this Fourier transformed space for the mth mode is,

$$\bar{K}_m(\nu, \tau) = \bar{K}_m(\nu - m\tau, 0). \tag{20}$$

This propagation to large values of ν in the Fourier transform leads to small scale structures in the velocity distribution; i.e., velocity space filamentation.

The development of filamentation on the velocity distribution, with its related propagation to large values of ν in the Fourier–Fourier transformed distribution, can lead to serious computational difficulty in the transformed space. To see this

consider Eq. (17). For the moment assume all the modes of σ are zero and consider the unfiltered limit, $\varepsilon = 0$. The elements of the matrix A contain the field mode amplitudes. In the dimensionless units being used [17] the field mode amplitudes are almost always quite small; assume this to be the case here. Then, for reasonable values of v, the $\bar{K}_m$ change slowly along their respective characteristics because the right side of Eq. (17) is small. In this case assume a numerical computation can be done on a reasonable grid. If, however, the $\bar{K}_m$ propagate to large v, then, from Eq. (17), they change rapidly along their characteristics even though the field mode amplitudes may still remain small. In this case, a finer grid becomes necessary to accommodate an accurate discrete computation. As the propagation to larger values of v occurs, the solution must be computed on a larger domain in the (v, τ) plane with a finer grid within it. The number of grid points on which the solution must be computed may grow rapidly, leading quickly to an intractable computation.

The practical solution in the past [2] to this problem has been to limit a computation to a finite fixed interval in v and hope that the information which propagates through the boundary of this interval, and is therefore lost, will not significantly influence the further evolution of the solution in the vicinity of $v = 0$ where the quantities of physical interest, the field mode amplitudes and the low order moments of the distribution function, are determined. In contrast, a filtered solution can be computed on a relatively small fixed interval in v with confidence that essentially no degradation of the solution accuracy in the vicinity of $v = 0$ will occur. From Eqs. (6) and (7), the relationship between the filtered and unfiltered K's is given by,

$$\bar{K}_m(v, \tau) = \pounds(v)\, K_m(v, \tau), \tag{21}$$

with

$$\pounds(v) = e^{-(1/2)(v/v_0)^2}, \tag{22}$$

and with v_0 defined by Eq. (19). Thus, because of the rapid decay of $\pounds(v)$ for $v \gg v_0$, truncation of the $\bar{K}_m$ at an appropriately large value of v can be carried out with assurance that the $\bar{K}_m$ will be as small as is necessary at the boundary to introduce negligible error elsewhere in the solution. In a computation of a filtered solution it is unnecessary to allow the domain of computation to expand in order to avoid the loss of significant information at the boundary of the domain; a filtered solution cannot propagate beyond several v_0. Further, since the domain does not expand, the need for a finer grid as the solution is computed is also avoided.

The method which is proposed here for overcoming the velocity space filamentation problem in the Fourier–Fourier transformed space is to compute solutions of the filtered Eqs. (17) through (19) on a fixed interval in v whose size is chosen large compared to v_0 so that the loss of information at the boundary of the interval is negligible. The price that is paid in using this method is the calculation of the extra diagonal terms in the matrix product on the right side of Eq. (17). In general this is

a small additional computation compared to the necessary convolution sum which must be done in any case. It appears that application of this filtering method to any approach for computing Vlasov solutions which involves a spatial Fourier series expansion of the distribution function would lead to a small additional computation effort per grid point. In the Fourier–Fourier transform approach the reduction in computation domain and the avoidance of unreasonably fine grids more than compensates for the extra computational effort which is needed.

IV. Examples

In this section two comparisons of one-dimensional unfiltered and filtered Vlasov–Maxwell solutions will be given; these are periodic solutions to Eqs. (17)–(19) with $\varepsilon = 0$ and $\varepsilon \neq 0$, respectively. The method used for generating these solutions is as discussed earlier by Klimas [17] except the computations are done on a fixed interval in v and the matrix, A, in the paper by Klimas is generalized to include the diagonal terms indicated on the right side of Eq. (17) when $\varepsilon \neq 0$. A discussion will be given of, first, a nonlinear Landau damping solution which exhibits strong velocity space filamentation, and second, a bump-on-tail unstable solution which exhibits weak filamentation only on a limited portion of the velocity distribution.

(a) *Nonlinear Landau Damping*

The nonlinear Landau damping solution which will be discussed has been considered by Klimas [17], by Cheng and Knorr [20], and by several other authors listed in Cheng and Knorr. This solution is characterized by an unusually strong initial field. The initial field energy in the plasma is equal to the initial thermal energy and it is carried in a single spatial Fourier mode, the fundamental mode, whose wavelength is the maximum in the plasma. The initial state of the plasma is specified by,

$$F(x, v, 0) = \sqrt{2\pi}\,(1 - \cos \pi x)\, e^{-(1/2)(2\pi v)^2}. \tag{23}$$

In the Fourier–Fourier transformed space, this initial state translates into,

$$K_0(v, 0) = e^{-(1/2)(v/2)^2}, \tag{24}$$

$$K_1(v, 0) = K_{-1}(v, 0) = \tfrac{1}{4} K_0(v, 0), \tag{25}$$

and all other $K_m(v, 0) = 0$. Thus, this is an initial state of the type described above as effectively a compact function of v in the transformed space.

Figure 1 shows the evolution of the real part of $K_1(v, \tau)$, a dominant Fourier mode in the solution, for $0 \leqslant \tau \leqslant 40$ and for $0 \leqslant v \leqslant 30$. After a short transient, the most important feature in this Fourier mode is the free streaming wave (in the sense of Eq. (20)) propagating, from the compact initial data, in the characteristic direc-

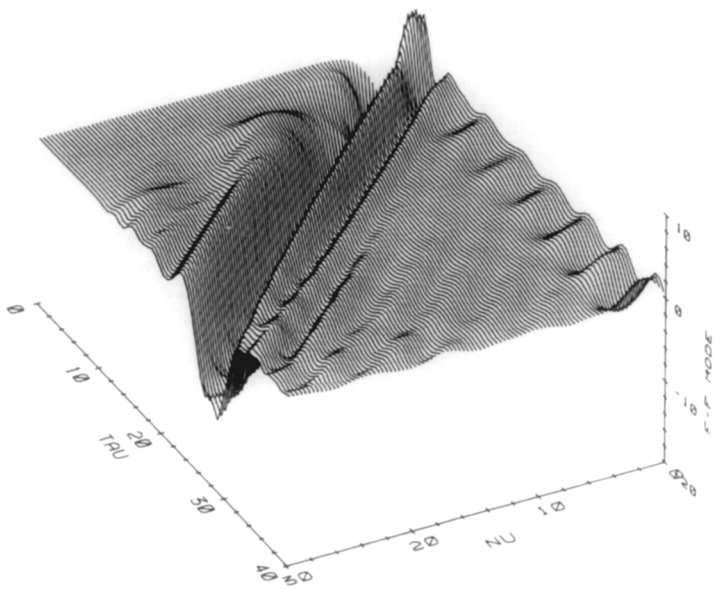

FIG. 1. Initial evolution of the real part of $K_1(v, \tau)$ for the unfiltered Landau damping solution.

tion of this mode. It is interesting that there is also a series of free streaming waves, following the first large one, which are not negligible in magnitude compared to the series of standing waves in the vicinity of $v = 0$. The physical description of the plasma is determined by the evolution of these standing waves in the "interaction region" near $v = 0$. For example, an electric field mode is given by the value of the related Fourier mode at $v = 0$ and all of the moments of a mode of the velocity distribution are given by the derivatives with respect to v, at $v = 0$, of the related Fourier mode. But, in Fig. 1 the Fourier mode itself is dominated by the free streaming components outside of the interaction region. This solution was computed on a fixed interval in v bounded by the cutoff at $v = 30$. It is clear that a significant amount of information has been lost through the cutoff boundary by the time $\tau = 40$. The consequences of this loss of information in the interaction region later in the solution are unknown.

The Fourier mode shown in Fig. 1 is part of an unfiltered solution. Now consider Fig. 2 which shows the same Fourier mode in a filtered version of the same solution. This is not to say that the Fourier mode shown in Fig. 2 was obtained by filtering that shown in Fig. 1. Figure 2 shows the real part of $\bar{K}_1(v, \tau)$ computed with Eqs. (17)–(19) using $v_0 = 5$ and using initial data related through Eqs. (21) and (22) to the unfiltered initial data given by Eqs. (24) and (25). In this case the large free streaming part of the Fourier mode has been suppressed while the standing waves in the interaction region have been left relatively unaffected. In the absence of the free streaming part of the mode very little information has been lost at the cutoff boundary where truncation of the solution is then acceptable; expan-

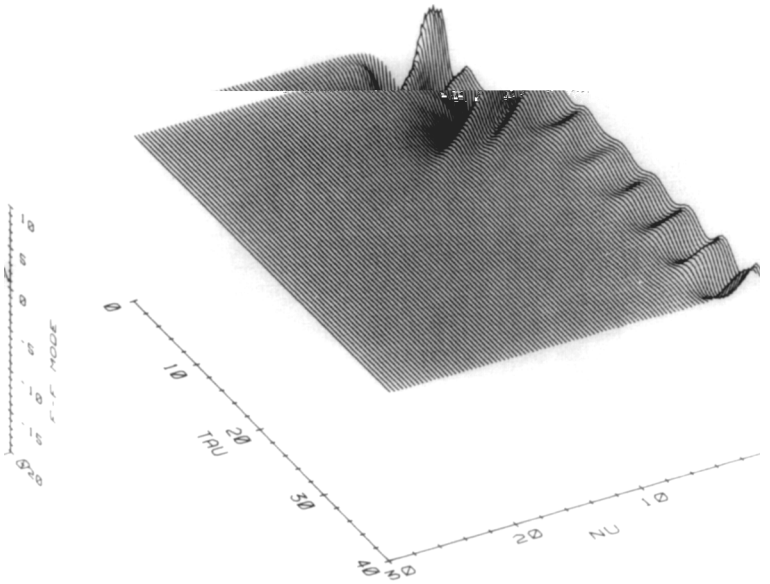

FIG. 2. Initial evolution of the real part of $K_1(v, \tau)$ for the filtered Landau damping solution.

sion of the computation domain to prevent information loss at the cutoff boundary is unnecessary. The relative simplicity of computing the filtered solution, compared to the unfiltered one, should be readily apparent following an examination of these two figures. Keep in mind, the Fourier mode shown in Fig. 1 is the slowest to expand of all the Fourier modes in the solution. The domain on which the unfiltered solution must be calculated, to assure the accuracy of the solution for large τ, is much larger than the one on which the filtered solution must be calculated. Furthermore, as discussed above, the grid which is used within the domain of computation for the filtered solution can be made much coarser than that used within the larger domain of computation associated with the unfiltered solution. The result is, the number of grid points on which the filtered solution must be computed is vastly reduced.

The filtered and unfiltered Fourier modes are related by Eqs. (21) and (22). Since $\mathfrak{L}(0) = 1$, the filtered and unfiltered Fourier modes should be identical at $v = 0$ and, therefore, the electric field modes calculated in either case should also be identical. Figures 3a and b provide a comparison between the fundamental field modes computed from a related pair of unfiltered and filtered nonlinear Landau damping solutions. The unfiltered solution is the one presented earlier by Klimas [17]; it is identical to the unfiltered solution discussed above except that it was computed on an expanding domain with no loss of information at the cutoff boundary. Consequently, the size of the computation domain and the number of grid points within it grew very large, the computation become unreasonably slow, and it was stopped at $\tau \simeq 41$. The filtered solution is the one discussed above. Over the range of τ in

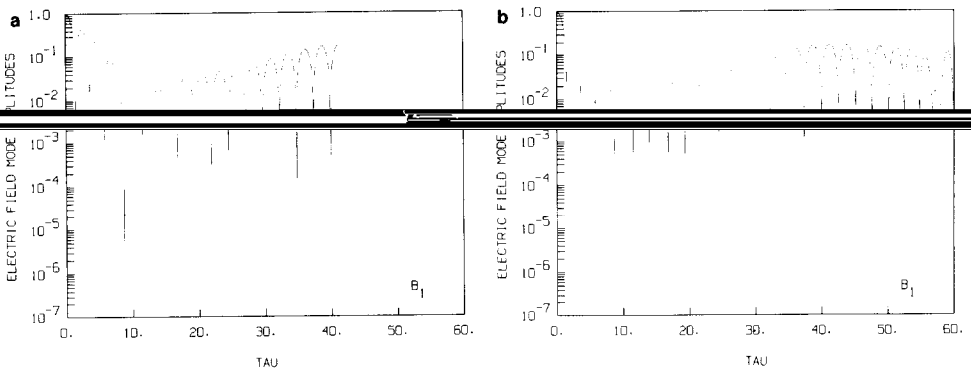

FIG. 3. Evolution with time of the absolute value of the fundamental field mode amplitude from the (a) unfiltered and (b) filtered Landau damping solution.

which the comparison can be made, it is difficult to find a difference in the two representations of the fundamental mode. The same can be said of the $m = 2$ mode shown in Figs. 4a and b. Figures 5a and b, which contain the $m = 4$ mode, show that some differences do sometimes emerge; this example is representative of the worst cases found so far. In general, when these differences have been found, they have been found in the relatively weak field modes. The accuracy demonstrated by Figs. 3a and b, as well as Figs. 4a and b, is representative of the results which have been found for the more dominant field modes.

Figures 6a and b provide a comparison of the space averaged ($m = 0$) velocity distributions computed from the unfiltered and filtered Landau damping solutions at $\tau = 35$. A comparison of Fig. 6a with the results of Cheng and Knorr [20], who used a very different integration method to obtain their results, shows that the complicated filamentation which has developed on the distribution has been computed accurately. The complexity of the distribution function shown in Fig. 6a is not an

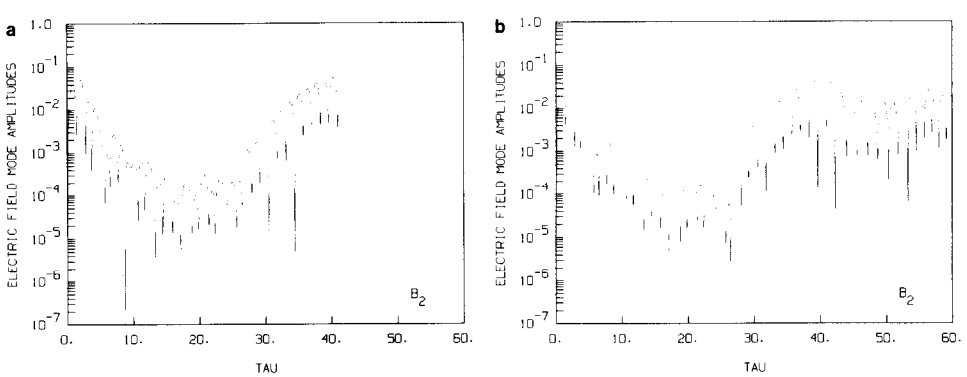

FIG. 4. Evolution with time of the absolute value of the $m = 2$ field mode amplitude from the (a) unfiltered and (b) filtered Landau damping solution.

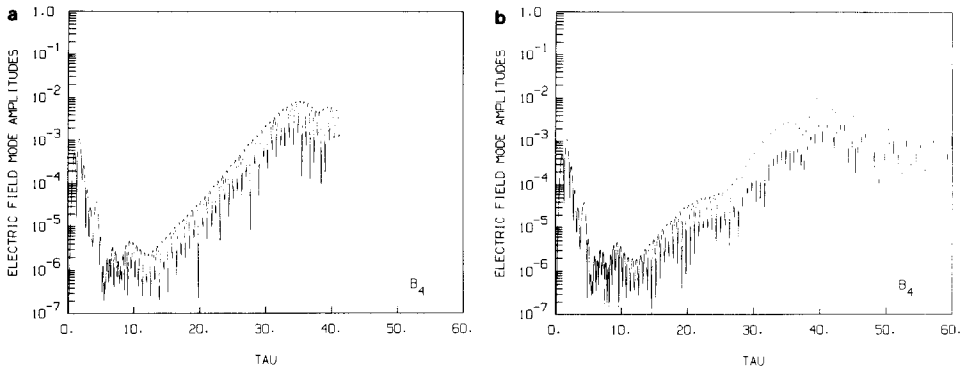

FIG. 5. Evolution with time of the absolute value of the $m = 4$ field mode amplitude from the (a) unfiltered and (b) filtered Landau damping solution.

artifact of the numerical integration; it is an accurate representation of a Vlasov solution. The choice, $v_0 = 5$, which was made to compute the filtered Landau damping solution, leads to a velocity space filter width, $v_0 = 0.064$. This width is sufficient to completely remove the filamentation from the velocity distribution and leave the smooth filtered distribution shown in Fig. 6b. In this case, a great deal of information has been lost. On the other hand, the result shown in Fig. 6b, rather than 6a, may be more representative of an experimental measurement of the velocity distribution using a detector with finite velocity resolution. It is not at all clear that smoothing away the filamentation has led to a less useful result. And, it should be remembered, the removal of the filamentation has not introduced any error in the computation of the Vlasov solution.

(b) *Bump-on-Tail Instability*

In the following, a comparison will be given between two filtered representations and one unfiltered representation of a bump-on-tail unstable Vlasov solution. The

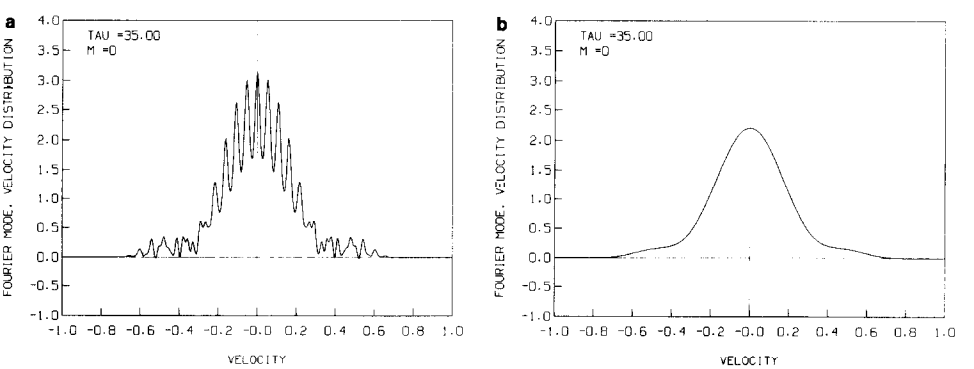

FIG. 6. Space averaged velocity distribution function for the (a) unfiltered and (b) filtered Landau damping solution at $\tau = 35$.

unfiltered solution has been discussed earlier by Klimas [24]; it was computed on a domain which generally expanded with the solution but which was occasionally cut back when this could be done with only a small loss of information at the cutoff boundary. Although this is not as desirable a comparison as that in the previous section where the unfiltered solution was computed with no loss of information, it is still considered a valid one because of the care which was exercised to minimize the loss of information. This is a periodic solution, therefore the quantity,

$$I(\tau) = \sum_m \int_{-v_c}^{v_c} dv \, |K_m(v, \tau)|^2, \tag{26}$$

should be a constant in τ for the unfiltered representation unless the solution propagates through the cutoff boundaries at $\pm v_c$ and is lost. For the unfiltered solution which will be discussed here $I(\tau)$ decreases with increasing τ due to the loss of information which occurred when the cutoff boundary was cut back. But, $I(\tau)$ was held to within 0.015% of its original value; the loss of information was kept small.

Figures 7a, b, and c show the initial space averaged velocity distributions which

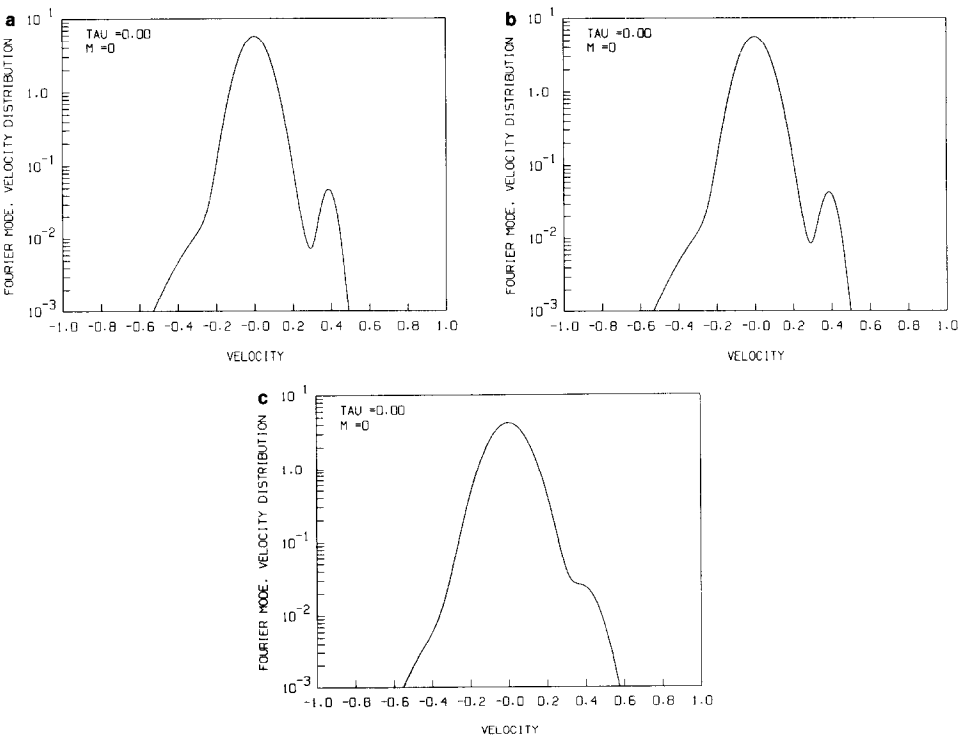

FIG. 7. Initial space averaged velocity distribution function for the (a) unfiltered, (b) first filtered, and (c) second filtered bump-on-tail solution.

were used for the unfiltered solution, the first filtered solution, and the second filtered solution respectively. The first filtered solution was computed using a narrow velocity filter ($v_0 = 0.016$; $v_0 = 20$) and the second filtered solution was computed using a broad velocity filter ($v_0 = 0.064$; $v_0 = 5$). The difference in velocity resolution is readily apparent in Figs. 7b and c. The first filtered initial distribution is visually close to the unfiltered initial distribution. But, the second initial distribution is considerably degraded. In this case the bump on the distribution has been almost completely removed, and the distribution looks as though it should be stable. It will be shown shortly that all three solutions exhibit the same unstable evolution. Earlier, it had been shown that the term on the right side of Eq. (8) acts as a diffusion operator when acting on a free streaming solution. In this case its behavior is very different. In a fascinating manner, that term somehow provides the information which is necessary to recognize the initial distribution shown in Fig. 7c as an unstable distribution even though the filtering of the initial distribution has apparently removed that information.

The evolution of the fundamental electric field mode for all three solutions is shown in Figs. 8a, b, and c. The phase velocity of this mode was adjusted so that it

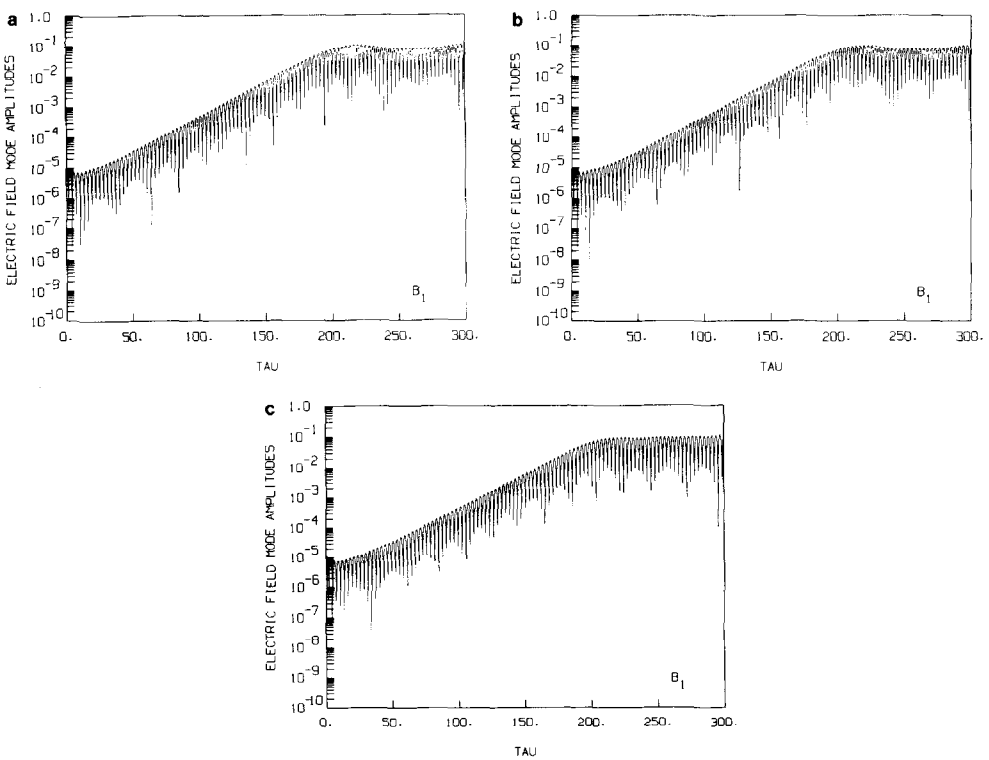

FIG. 8. Evolution with time of the absolute value of the fundamental field mode amplitude from the (a) unfiltered, (b) first filtered, and (c) second filtered bump-on-tail solution.

lies on the rising portion of the bump on the initial unfiltered space averaged velocity distribution. Thus, this mode exhibits the classical initial transient, leading to linear growth, and then to saturation due, in this case, to trapping. Note that all three solutions are in excellent agreement, they all obviously exhibit the same unstable evolution, including the second filtered solution which, as discussed in the previous paragraph, follows from an initial state that does not appear unstable.

The evolution of the next mode ($m = 2$) for all three solutions is shown in Figs. 9a, b, and c. The initial phase velocity of this mode lies on the core of the distribution, and so, it Landau damps. However, at $\tau \simeq 70$ the amplitude of this mode becomes so small, while the amplitude of the growing fundamental mode has grown so large, second order wave–wave coupling begins to dominate the linear wave–particle interaction and this mode reverses its evolution to grow at twice the growth rate and with twice the frequency of the fundamental mode. Saturation of this mode occurs when the fundamental mode saturates. All three representations of this mode are in excellent agreement over the course of this evolution. Only the second filtered solution, with its broad velocity space filter, differs slightly following saturation. Higher order, less significant, modes have been found to exhibit similar agreement; excellent up to saturation and then small differences in detail.

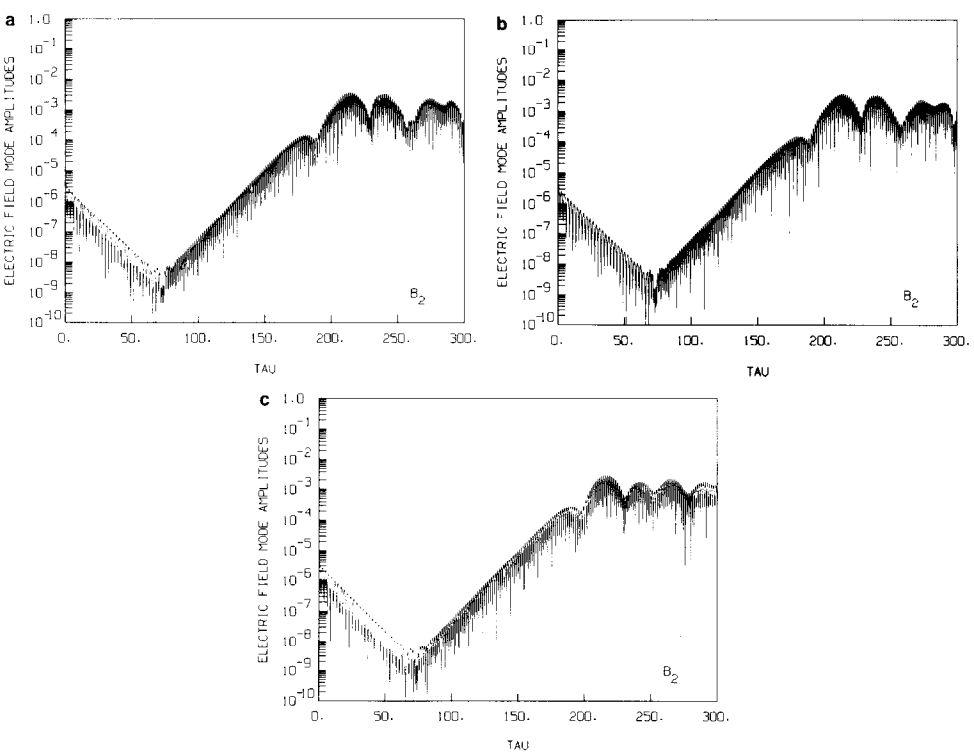

FIG. 9. Evolution with time of the absolute value of the $m = 2$ field mode amplitude from the (a) unfiltered, (b) first filtered, and (c) second filtered bump-on-tail solution.

Figures 10a, b, and c show the space averaged velocity distribution functions for all three solutions at $\tau = 200$. At this time the instability is just about to saturate. The unfiltered representation shows that the bump on the distribution has been reduced considerably. The only evidence for velocity space filamentation in this solution can be found here superposed on the remaining portion of the bump. This filamentation persists in this region of velocity for as long as the solution has been computed (up to $\tau = 600$) but never develops elsewhere. Nevertheless, unless a very clever numerical code were developed, a relatively fine velocity grid over all significant values of velocity, or as in this case, a relatively large computation domain in the transformed space, is necessary to compute this solution accurately. Figure 10b shows that the narrow width of the velocity filter used to obtain the first filtered solution leaves the smooth portions of this velocity distribution relatively unchanged but it does smooth away the filamentation in the vicinity of the bump. Thus, for this solution, were it being computed in velocity space, a coarser grid appropriate for the majority of the distribution would be more appropriate. Figure 10c shows that the second filtered velocity distribution has hardly evolved, and that it still fails to exhibit much information. Even so, this kind of solution can be useful in situations where the field output is sufficient to determine whether or not a more

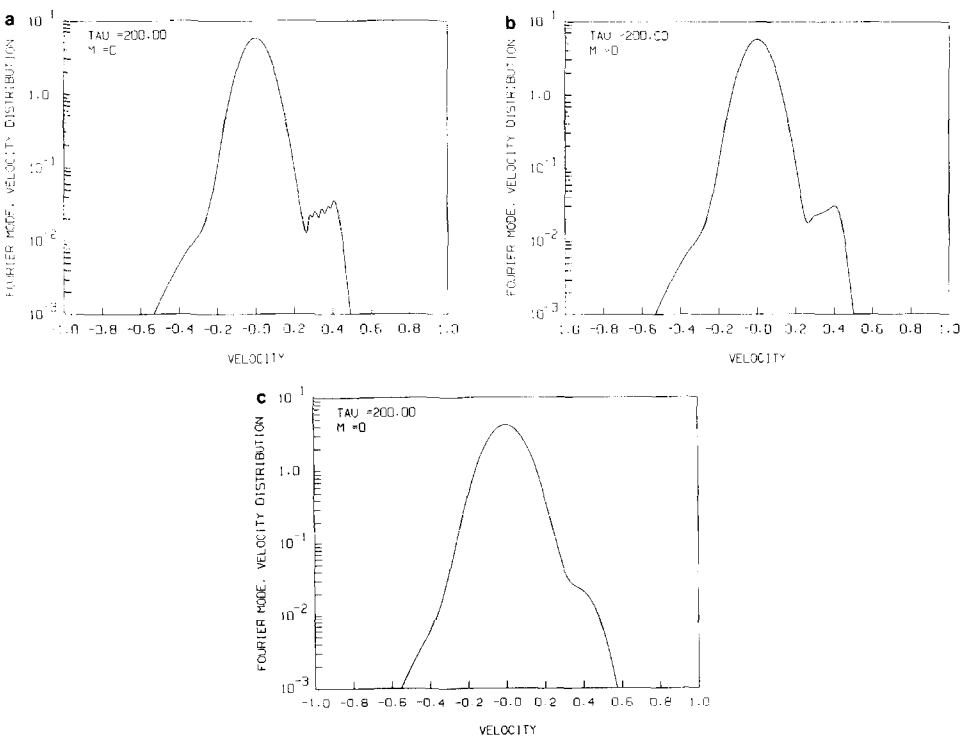

FIG. 10. Space averaged velocity distribution function for the (a) unfiltered, (b) first filtered, and (c) second filtered bump-on-tail solution at $\tau = 200$.

detailed examination is warranted. For example, a sequence of solutions calculated with the variation of a parameter could be done quickly to find cases which might exhibit a particular physical behavior and, therefore, be chosen for further study.

V. Discussion

It is unfortunate that a direct comparison of the several examples given in the previous section for relative running speeds cannot be done. The older unfiltered solutions were computed on an IBM 360-91 while the new filtered solutions were computed on an IBM 3081. Nevertheless, various pieces of information can be combined to construct a reasonably reliable estimate of the relative running speeds which would have been attained if the computations had all been done on the same machine.

Following installation, the IBM 3081 was tested for running speed, relative to the IBM 360-91, using a variety of numerical codes. It was found that the running speeds, while depending on the particular code, were approximately equal. If the assumption is made that the running speeds for the two machines are equal for the codes under consideration here, then it can be concluded the unfiltered Landau damping solution took approximately a factor of ten longer to compute than the filtered Landau damping solution and the run times for the unfiltered, first filtered, and second filtered bump-on-tail solutions are approximately in the ratios 11:3:1. These run time ratios are probably quite close to the ratios which would have been found if these solutions were all obtained on the same computer; they are corroborated by other considerations. For example, an estimate of the relative run times can be made by simply comparing the number of grid points which were necessary to compute the unfiltered and filtered solutions. The numbers of grid points for the two Landau damping solutions are in the ratio 12:1, and the numbers for the bump-on-tail solutions are in the ratios 14:4:1. These ratios are in reasonable agreement with those attained by simply comparing run times for the different computations ignoring the change in computers. Further, the relative run times and number of grid points for the two filtered bump-on-tail solutions, which were both computed on the same computer, can be compared. The relative run times are in the ratio 2.5:1 while the relative number of grid points are in the ratio 3.1:1. Thus, this method of estimating the relative run times using the relative number of grid points seems reasonably accurate. It appears that approximately a factor of ten increase in computation speed can be expected unless a narrow velocity filter is used to preserve some of the finer detail in the velocity distribution function.

Considerable savings in real machine memory can be attained by computing the filtered solutions in lieu of the unfiltered ones. Assuming that the solution is computed by marching forward in time with only a few time steps retained in machine memory at any point in the computation, then the amount of storage required for an unfiltered solution, relative to a filtered solution, is determined by the ratio of the widths, in v, of the two computation domains as well as, of course, the grid

spacing within the computation domains. The unfiltered bump-on-tail solution required 8 times the memory necessary for the first filtered solution, with its narrow velocity filter, and it required 25 times the memory necessary for the second filtered solution. For the Landau damping solutions this ratio got as large as 30 before the computation of the unfiltered solution was finally stopped. The computation of the filtered Landau damping solution was done with approximately 300 grid points per time step per spatial Fourier model. Certainly, fewer grid points were necessary. Figures 1 and 2 can be examined to see the resolution of the unfiltered and filtered solutions which was attained. In those figures, of the grid points on which the solutions were actually computed only every eighth in v and every sixteenth in τ are plotted.

VI. Conclusion

A method for overcoming the velocity space filamentation problem in collisionless plasma models has been introduced. In this method solutions of the filtered Vlasov–Maxwell equations, in lieu of the Vlasov–Maxwell equations themselves, are computed. It has been shown that this method introduces no error in the Vlasov–Maxwell solutions, it yields the exact field solutions with no modifications, and it produces filtered velocity distribution functions. It has been further shown that with an appropriate choice of filter width velocity space filamentation cannot develop in the filtered solutions. It has been also conjectured that position space filamentation will not develop in the filtered solutions.

Several computations of both unfiltered and filtered solutions have been discussed. The comparisons of these unfiltered and filtered solutions which have been made show that the method presented here for overcoming the velocity space filamentation problem is an attractive one in practice. The computed field solutions, for the unfiltered and filtered solutions, agree in considerable detail with each other. The velocity distribution functions computed using the filtered equations are indeed filtered representations of the solutions computed using the unfiltered equations; i.e., the method, in practice, does not introduce noticeable error in the evolution of the velocity distribution. Finally, large reductions in computation time and computer memory requirements have been demonstrated.

APPENDIX A: Generalization to an Electromagnetic Field in Three Dimensions

In this Appendix the filtered Vlasov–Maxwell equations will be constructed for a distribution function and electromagnetic field in three dimensions. The results will be similar to those given above for the one-dimensional electron plasma model. It will be shown that the filtered equations are exactly the same system of equations as the unfiltered ones except for the addition of a single term on the right side of the

Vlasov equation which is a generalization of the one-dimensional scalar form of this term given above. The electromagnetic field will be shown to be invariant to the filtering process and the absence of velocity space filamentation on the filtered velocity distribution will be demonstrated.

The filter function which is used to construct the filtered distribution function should always be an even function of velocity with unit integrated weight in whatever number of dimensions are involved. In this appendix a simple gaussian will be used; in Appendix B more general filter functions will be discussed. Therefore, in this case,

$$\mathfrak{L}(\mathbf{v}) = (1/v_0\sqrt{2\pi})^3\, e^{-(1/2)(\mathbf{v}\cdot\mathbf{v}/v_0^2)}, \tag{A1}$$

with the consequence,

$$\mathbf{v}\mathfrak{L}(\mathbf{v}) = -v_0^2 \frac{\partial \mathfrak{L}(\mathbf{v})}{\partial \mathbf{v}}. \tag{A2}$$

The filtered velocity distribution is defined through

$$\begin{aligned} \bar{F}(\mathbf{v}) \equiv \mathfrak{L} * F &\equiv \int d^3v'\, \mathfrak{L}(\mathbf{v}-\mathbf{v}')\, F(\mathbf{v}') \\ &= \int d^3v'\, \mathfrak{L}(\mathbf{v}')\, F(\mathbf{v}-\mathbf{v}'), \end{aligned} \tag{A3}$$

in which only the velocity dependence of the distribution functions has been explicitly exhibited. Just as in the one-dimensional case, an a priori bound can be placed on the derivative of $\bar{F}$ with respect to velocity thereby precluding the development of filamentation. Let $\hat{a}$ be an arbitrary unit vector and consider,

$$\hat{a}\cdot\frac{\partial \bar{F}(\mathbf{v})}{\partial \mathbf{v}} = \int d^3v' \left(\hat{a}\cdot\frac{\partial \mathfrak{L}(\mathbf{v}-\mathbf{v}')}{\partial \mathbf{v}}\right) F(\mathbf{v}'). \tag{A4}$$

This is the derivative with respect to velocity of $\bar{F}$ in an arbitrary direction. Using the method outlined above for obtaining Eq. (12) from Eq. (11), it can be shown that,

$$\left|\hat{a}\cdot\frac{\partial \bar{F}(\mathbf{v})}{\partial \mathbf{v}}\right| \leqslant \bar{F}_{\mathrm{m}}/v_0\sqrt{2\pi}, \tag{A5}$$

in which $\bar{F}_{\mathrm{m}}$ is the maximum value of $\bar{F}$ which is imposed on the solution in the initial or boundary data. The maximum velocity derivative which can occur in the filtered solution can be estimated and adjusted, through the choice of the parameter v_0, before computing the solution. The degree to which filamentation is allowed to develop can be controlled by the choice of v_0.

The starting point for the construction of the filtered equations is the Vlasov equation,

$$\frac{\partial F}{\partial t}+\mathbf{v}\cdot\frac{\partial F}{\partial \mathbf{x}}-\frac{e}{m}\left(\mathbf{E}+\frac{\mathbf{v}}{c}\times\mathbf{B}\right)\cdot\frac{\partial F}{\partial \mathbf{v}}=0, \tag{A6}$$

for the electron velocity distribution function, plus Maxwell's equations for the electromagnetic field. (If other particle species were included, then the calculation which will be done in the following could also be done with no changes for a mul-

and has unit weight under integration over velocity, the zeroth and first moments of the velocity distribution are invariant to filtering; i.e.,

$$\int d^3v\, F(\mathbf{x}, \mathbf{v}, t)=\int d^3v\, \bar{F}(\mathbf{x}, \mathbf{v}, t) \tag{A7}$$

and

$$\int d^3v\, \mathbf{v}F(\mathbf{x}, \mathbf{v}, t)=\int d^3v\, \mathbf{v}\bar{F}(\mathbf{x}, \mathbf{v}, t). \tag{A8}$$

Thus, the charge and current densities which enter Maxwell's equations can be computed using the filtered velocity distribution or the unfiltered one with no change in the results. Maxwell's equations, and the field solutions, are unaffected by the shift to the filtered velocity distribution function.

The filtered Vlasov equation is constructed by applying the convolution integration exhibited in Eq. (A3) to the Vlasov equation. This treatment of the first term in the Vlasov equation quickly yields,

$$\pounds * \frac{\partial F}{\partial t}=\frac{\partial \bar{F}}{\partial t}. \tag{A9}$$

From the second term,

$$\pounds * \mathbf{v}\cdot\frac{\partial F}{\partial \mathbf{x}}=\mathbf{v}\cdot\frac{\partial \bar{F}}{\partial \mathbf{x}}-\int d^3v'\, \pounds(\mathbf{v}')\, \mathbf{v}'\, F(\mathbf{v}-\mathbf{v}'). \tag{A10}$$

It is at this point that the choice of a gaussian for the filter function becomes crucial. With this choice, the integral term in this equation can be reduced further to a simple form involving $\bar{F}$ and not F. Then, the filtered Vlasov–Maxwell equations become a closed system for $\bar{F}$ and the electromagnetic field. In Appendix B more general filter functions will be discussed, but the generalizations considered will be limited to retain this property. With the gaussian choice Eq. (A2) can be used to reduce Eq. (A10) to,

$$\pounds * \mathbf{v}\cdot\frac{\partial F}{\partial \mathbf{x}}=\mathbf{v}\cdot\frac{\partial \bar{F}}{\partial \mathbf{x}}+v_0^2\left(\frac{\partial}{\partial \mathbf{x}}\cdot\frac{\partial}{\partial \mathbf{v}}\right)\bar{F}, \tag{A11}$$

a differential form acting on $\bar{F}$ only. From the third term in the Vlasov equation, involving the electric field, it is easy to show that,

$$\pounds * \mathbf{E} \cdot \frac{\partial F}{\partial \mathbf{v}} = \mathbf{E} \cdot \frac{\partial \bar{F}}{\partial \mathbf{v}}. \tag{A12}$$

Finally, from the fourth term,

$$\begin{aligned} \pounds * (\mathbf{v} \times \mathbf{B}) \cdot \frac{\partial F}{\partial \mathbf{v}} &= (\mathbf{v} \times \mathbf{B}) \cdot \frac{\partial \bar{F}}{\partial \mathbf{v}} \\ &\quad - \int d^3v' \, \pounds(\mathbf{v}')(\mathbf{v}' \times \mathbf{B}) \cdot \frac{\partial F(\mathbf{v} - \mathbf{v}')}{\partial \mathbf{v}}. \end{aligned} \tag{A13}$$

Once again, the choice of gaussian filter function is crucial for reducing the integral term in this equation further and the more general filter functions which will be discussed in Appendix B will be chosen to retain the reduction about to be attained here. With Eq. (A2), this integral term can be rewritten as,

$$v_0^2 \int d^3v' \left(\mathbf{B} \times \frac{\partial \pounds(\mathbf{v}')}{\partial \mathbf{v}} \right) \cdot \frac{\partial F(\mathbf{v} - \mathbf{v}')}{\partial \mathbf{v}'}, \tag{A14}$$

and then, through integration by parts, as,

$$-v_0^2 \int d^3v' \, \pounds(\mathbf{v}') \left(\mathbf{B} \times \frac{\partial}{\partial \mathbf{v}'} \right) \cdot \frac{\partial F(\mathbf{v} - \mathbf{v}')}{\partial \mathbf{v}'}, \tag{A15}$$

which always yields a zero because, the differential operator,

$$\left(\mathbf{B} \times \frac{\partial}{\partial \mathbf{v}'} \right) \cdot \frac{\partial}{\partial \mathbf{v}'}, \tag{A16}$$

yields zero when acting on any differentiable function of $\mathbf{v}'$. Thus, the rather surprising result,

$$\pounds * (\mathbf{v} \times \mathbf{B}) \cdot \frac{\partial F}{\partial \mathbf{v}} = (\mathbf{v} \times \mathbf{B}) \cdot \frac{\partial \bar{F}}{\partial \mathbf{v}}, \tag{A17}$$

and finally, the filtered Vlasov equation,

$$\begin{aligned} &\frac{\partial \bar{F}}{\partial t} + \mathbf{v} \cdot \frac{\partial \bar{F}}{\partial \mathbf{x}} - \frac{e}{m} \left(\mathbf{E} + \frac{\mathbf{v}}{c} \times \mathbf{B} \right) \cdot \frac{\partial \bar{F}}{\partial \mathbf{v}} \\ &\qquad = -v_0^2 \left(\frac{\partial}{\partial \mathbf{x}} \cdot \frac{\partial}{\partial \mathbf{v}} \right) \bar{F}. \end{aligned} \tag{A18}$$

The simplicity of this result is remarkable. Equations (A6) and (A18) should be compared to see the modification of the Vlasov–Maxwell system of equations which occurs under filtration. Maxwell's equations, and the field solutions, are unchanged while a single differential term is added to the right side of the Vlasov equation. If the initial and boundary data for F and $\bar{F}$ are chosen to satisfy Eq. (A3), then this additional term acts to ensure the solutions of Eqs. (A6) and (A18) also satisfy Eq. (A3).

APPENDIX B: GENERALIZED FILTER FUNCTIONS

Cheng [22] and Knorr [23] have pointed out that alternative theories for velocity-filtered distribution functions can be developed by using other than the simple gaussian filter functions which have been employed in this paper. Their ideas for producing these alternative theories will be discussed here. It is beyond the scope of this paper to determine the most general acceptable filter function. Instead, the possibility of generalization will be demonstrated and, in particular, it will be shown that the filter function which Cheng and Knorr used in their related work [20] is one of the possible generalizations.

To retain the property that the field portion of a Vlasov–Maxwell solution be unaffected by the transition to the filtered Vlasov–Maxwell solution it is merely necessary to restrict the choice of filter function to one that is even in velocity and has unit weight under velocity integration. The more difficult restrictions on the choice of filter function follow from the decision to retain, as far as possible, the simplicity of the results which have been attained in Appendix A using the gaussian filter function. In particular, the result shown in Eq. (A17) as well as the reduction of the integral term shown in Eq. (A10) to a form similar to that shown in Eq. (A11) should be required. Then the filtered Vlasov–Maxwell equations would once again be identical to their unfiltered counterparts except for the addition of a single term on the right side of the Vlasov equation which would operate solely on $\bar{F}$, not F. It is the property of the gaussian function given by Eq. (A2) which assures this result. A possible generalization of Eq. (A2) is given by,

$$\mathbf{v}\mathfrak{L}(\mathbf{v}) = -\alpha \frac{\partial}{\partial \mathbf{v}} \left(\frac{\partial}{\partial \mathbf{v}} \cdot \frac{\partial}{\partial \mathbf{v}} \right)^{n-1} \mathfrak{L}(\mathbf{v}), \tag{B1}$$

in which α is a constant parameter and n is any positive integer greater than zero; the special case given by Eq. (A2) can be regained by setting $n = 1$. With this generalization, Eq. (A11) is replaced by,

$$\begin{aligned} \mathfrak{L} * \mathbf{v} \cdot \frac{\partial F}{\partial \mathbf{x}} = \mathbf{v} \cdot \frac{\partial \bar{F}}{\partial \mathbf{x}} \\ + \alpha \left(\frac{\partial}{\partial \mathbf{x}} \cdot \frac{\partial}{\partial \mathbf{v}} \right) \left(\frac{\partial}{\partial \mathbf{v}} \cdot \frac{\partial}{\partial \mathbf{v}} \right)^{n-1} \bar{F}, \end{aligned} \tag{B2}$$

and Eq. (A17) is unchanged. Therefore, in terms of the goals specified above this is an appropriate generalization. The properties of the filter functions which are the solutions of Eq. (B1) can be best understood by considering their Fourier transforms. Equation (B1) can be Fourier transformed and, with an appropriate adjustment to α, the result can be written as,

$$\frac{\partial \mathfrak{L}(\mathbf{v})}{\partial(\mathbf{v}/v_0)} = -n\left(\frac{\mathbf{v}}{v_0}\right)\left(\frac{\mathbf{v}}{v_0}\cdot\frac{\mathbf{v}}{v_0}\right)^{n-1}\mathfrak{L}(\mathbf{v}), \tag{B3}$$

in which $\mathbf{v}$ is the Fourier variable. Due to the restriction to unit weight filter functions, the solution of Eq. (B3) which is desired is given by,

$$\mathfrak{L}(\mathbf{v}) = e^{-(1/2)}\left(\frac{\mathbf{v}}{v_0}\cdot\frac{\mathbf{v}}{v_0}\right)^{n}. \tag{B4}$$

Again, the choice $n=1$ leads to the gaussian filter function which has been discussed in this paper in both one and three dimensions. In one dimension, the choice $n=2$ leads to the filter function used by Cheng and Knorr [20].

The higher order filter functions obtained with increasing n have the disadvantage that as n increases so does the order of the differential operator which is given in Eq. (B2) and which will ultimately appear on the right side of the Vlasov equation. However, the higher order filter functions are also attractive in some ways. For any given value of n, all of the velocity moments of F, from moment zero through moment $2n-1$, are invariant to the filtering process. This invariance could be advantageous in situations where the moment expansion of F is significant. Further, in the Fourier transformed velocity space the more rapid decrease of the filter function with increasing magnitude of v which is attained with larger values of n makes the propagation of information to large values of v even more difficult than in the case of a gaussian filter function. For these reasons it is thought that the higher order filter functions should be investigated in the future. At present, no other generalizations of the filter function which satisfy the requirements stated above have been found.

Acknowledgments

It is a pleasure to acknowledge the suggestions of C. Z. Cheng and G. Knorr who both pointed out the existence of generalizations to the gaussian filter function used in this study. Special thanks to all of the members of the NASA Space and Earth Sciences Computing Center and the Information Analysis and Display Office for their invaluable assistance. My deepest appreciation to A. K. Tolbert.

References

1. J. Denavit, *J. Comput. Phys.* **9**, 75 (1972).
2. T. P. Armstrong, R. C. Harding, G. Knorr, and D. Montgomery, in *Methods in Computational Physics*, Vol. 9, edited by S. Fernbach *et al.* (Academic Press, New York, 1970), p. 29.

3. G. KNORR, *Z. Naturforsch. A* **16**, 1320 (1961).
4. P. J. KELLOGG, *Phys. Fluids* **8**, 102 (1965).
5. F. C. GRANT AND M. R. FEIX, *Phys. Fluids* **10**, 696 (1967).
6. F. C. GRANT AND M. R. FEIX, *Phys. Fluids* **10**, 1356 (1967).
7. T. P. ARMSTRONG AND D. MONTGOMERY, *J. Plasma Phys.* **1**, 425 (1967).
8. T. P. ARMSTRONG, *Phys. Fluids* **10**, 1269 (1967).
9. T. P. ARMSTRONG AND D. MONTGOMERY, *Phys. Fluids* **12**, 2094 (1969).
10. G. JOYCE, G. KNORR, AND T. BURNS, *Phys. Fluids* **14**, 797 (1971).
11. G. KNORR, *J. Comput. Phys.* **13**, 165 (1973).
12. G. JOYCE, G. KNORR, AND H. K. MEIER, *J. Comput. Phys.* **8**, 53 (1971).
13. G. KNORR, *Z. Naturforsch. A* **18**, 1304 (1963).
14. J. DENAVIT, B. W. DOYLE, AND R. H. HIRSCH, *Phys. Fluids* **11**, 2241 (1968).
15. J. DENAVIT, in *Proceedings of the Fourth Conference on Numerical Simulation of Plasma*, edited by J. P. Boris and R. H. Shanny (Naval Research Laboratory, 1970), p. 305.
16. J. DENAVIT AND W.L. KRUER, *Phys. Fluids* **14**, 1782 (1971).
17. A. J. KLIMAS, *J. Comput. Phys.* **50**, 270 (1983).
18. R. W. GOULD, T. M. O'NEIL, AND J. H. MALMBERG, *Phys. Rev. Lett.* **19**, 219 (1967).
19. T. M. O'NEIL AND R. W. GOULD, *Phys. Fluids* **11**, 134 (1968).
20. C. Z. CHENG AND G. KNORR, *J. Comput. Phys.* **22**, 330 (1976).
21. A. J. KLIMAS AND J. COOPER, *Phys. Fluids* **26**, 478 (1983).
22. C. Z. CHENG, personal communication (September 1985).
23. G. KNORR, personal communication (September, 1985).
24. A. J. KLIMAS, *J. Geophys. Res.* **88**, 9081 (1983).